Earth and Planetary Science Letters 305 (2011) 425–434

Contents lists available at ScienceDirect

Earth and Planetary Science Letters

journal homepage: www.elsevier.com/locate/epsl

Partitioning behavior at 9 GPa in the Fe–S system and implications for planetary evolution

Nancy L. Chabot [a,*], William F. McDonough [b], John H. Jones [c], Sarah A. Saslow [d], Richard D. Ash [b], David S. Draper [c], Carl B. Agee [e]

[a] Johns Hopkins University Applied Physics Lab, 11100 Johns Hopkins Rd, Laurel, MD, 20723, United States
[b] University of Maryland, College Park, MD, 20742, United States
[c] NASA Johnson Space Center, Houston, TX, 77058, United States
[d] Northwestern University, Evanston, IL, 60208, United States
[e] University of New Mexico, Albuquerque, NM, 87131, United States

ARTICLE INFO

Article history:
Received 23 November 2010
Received in revised form 14 March 2011
Accepted 17 March 2011
Available online 11 April 2011

Editor: R.W. Carlson

Keywords:
siderophile elements
Fe–FeS
high pressure experiments
solid metal–liquid metal partitioning
iron
sulfur

ABSTRACT

Solid metal/liquid metal partitioning experiments were conducted at 9 GPa and 1323–1873 K in the Fe–S system. Analysis of the experimental charges by *in situ* laser ablation inductively coupled plasma mass spectrometry enabled partitioning results to be obtained for a total of 21 trace elements (Co, Ni, Cu, Ga, Ge, As, Mo, Ru, Rh, Pd, Ag, Sn, Sb, W, Re, Os, Ir, Pt, Au, Pb, and Bi). This new, elevated pressure dataset for the Fe–S system allows a direct comparison to the extensive data available at 0.1 MPa and permits evaluation of the effect of pressure on partitioning in this system. The majority of the elements studied exhibit different solid metal/liquid metal partitioning behaviors at 9 GPa than at 0.1 MPa. Additionally, the nature of these differences varies significantly between the 21 trace elements studied, spanning the range of behaviors of partitioning from more strongly into solid metal, to less strongly into solid metal, and to becoming insensitive to the metallic liquid composition. We conclude that pressure affects solid metal/liquid metal partitioning behavior in the Fe–S system and discuss the implications for fractionations due to Earth's core solidification and for planetary differentiation models.

1. Introduction

Understanding the partitioning behavior of trace elements is key to interpreting and predicting compositional signatures produced by differentiation and evolutionary processes in planetary bodies. In particular, the partitioning results from solid metal/liquid metal experiments in the Fe–S system have been used to model and understand the crystallization history of iron meteorites (e.g. Chabot and Haack, 2006) and to unravel the genesis of other meteorites, such as ureilites (Rankenburg et al., 2008; Warren et al., 2006) and enstatite chondrites (Humayun et al., 2009; van Niekerk et al., 2009). The histories of meteorites and the differentiation of meteorite parent bodies do not involve elevated pressures, so the use of experimental solid metal/liquid metal partitioning data acquired at the condition of atmospheric pressure is directly applicable to these cases. A large amount of solid metal/liquid metal partitioning data is available in the Fe–S system from experiments conducted at atmospheric conditions, and such data are available for over 25 different trace elements relevant to metallic systems (e.g. summarized in Chabot et al., 2003, 2009). The experimental studies at atmospheric pressure indicate that the amount of S present in the metallic liquid can have a significant influence on the partitioning behavior of trace elements and that the presence of S affects elements differently, creating fractionations between trace elements during metal solidification or melting in the Fe–S system. Unlike the large amount of data available at atmospheric pressure, only a handful of studies have explored the effect of pressure on solid metal/liquid metal partitioning behaviors in the Fe–S system.

The earliest study was by Jones and Walker (1991), whose two experiments at 8 GPa suggested a slight pressure effect for Ge but no such effect for Au, Ni, or P. Nine years later, Walker (2000) reported results for Pt, Re, Os, and Ni at 10 GPa that did not suggest a pressure effect on the solid metal/liquid metal partitioning of Pt, Re, or Os but did have Ni partitioning values that differed from 0.1 MPa results. However, the differences in the Ni partitioning results were attributed to the high levels of Pt, Re, and Os in the experiments rather than being due to the elevated pressure. A few years later, Lazar et al. (2004) followed with results for Ni, Mo, Ru, Re, Tc, and Ti at 6 GPa and found a distinct effect of pressure on the partitioning behavior of Mo in particular. Lazar et al. (2004) concluded that their Ni values were generally consistent with the previously published 0.1 MPa values, though close inspection of their Fig. 4b shows a slight deviation between the 0.1 MPa and 6 GPa data at higher S contents. Lazar et al.

* Corresponding author.
E-mail address: nancy.chabot@jhuapl.edu (N.L. Chabot).

0012-821X/$ – see front matter © 2011 Elsevier B.V. All rights reserved.
doi:10.1016/j.epsl.2011.03.027

(2004) also concluded that their data at 6 GPa for Re and Ru were consistent with the 0.1 MPa partitioning values for these elements, though at the time, 0.1 MPa data for Ru were limited to two determinations. Motivated by the difference between Mo solid metal/liquid metal partitioning at 0.1 MPa and 6 GPa discovered by Lazar et al. (2004), Walker and Li (2008) conducted a systematic study of the partitioning of Mo in the Fe–S system at constant temperature and bulk composition from 0.1 MPa to 4 GPa. Their Mo partitioning results fell between the 6 GPa data of Lazar et al. (2004) and the data from 0.1 MPa studies, confirming the effect discovered by Lazar et al. (2004). However, Walker and Li (2008) ascribed the changing partitioning behavior of Mo not to a pressure effect but rather as a result of the liquidus surface shape of the Fe–S system in this pressure range. Walker and Li (2008) predicted that the reason Mo, but not Ru or Re, was exhibiting this changing partitioning behavior was due to the marginally siderophile nature of Mo and its slightly chalcophile tendencies, in contrast to more siderophile elements.

More recently, two studies have focused on the solid metal/liquid metal partitioning behavior of Pt, Re, and Os at elevated pressures (Hayashi et al., 2009; Van Orman et al., 2008). The interest in these particular elements arises from the discovery of enriched ^{186}Os and ^{187}Os isotopes in basalts and their inferred mantle–plume sources and the suggestion that these more radiogenic Os isotopic compositions may be due to core–mantle exchange (e.g. Brandon and Walker, 2005; Walker et al., 1995). To create the observed signature, Earth's core must fractionate Pt, Re, and Os between the solid inner core and the liquid outer core, with the outer liquid core enriched in Pt and Re relative to Os. Van Orman et al. (2008) reported results for three experiments at 3 GPa, two experiments at 18 GPa, and one experiment at 22 GPa. By comparing the 3 GPa results with the combined 18 and 22 GPa results, they concluded that the solid metal/liquid metal partition coefficients for Pt, Re, and Os all decreased with increasing pressure and became more similar to each other. Such a decrease with pressure would not enrich Earth's outer core in Pt and Re relative to Os to the levels required to match the mantle plume sources. Hayashi et al. (2009) conducted nine experiments ranging from 5 to 20 GPa and, in contrast to Van Orman et al. (2008), they found no significant effect of pressure on the solid metal/liquid metal partition coefficients of Pt, Re, or Os. Hayashi et al. (2009) noted that their runs were Ni-bearing, in contrast to the experiments of Van Orman et al. (2008), and suggested that the presence of Ni could have caused the discrepancy between the two studies. However, the experiments of Hayashi et al. (2009) report a maximum Ni content of 19 wt.% and the majority of the experimental run products have Ni contents <9 wt.%; such low Ni contents are unlikely to cause the difference found for the effect of pressure on the solid metal/liquid metal partitioning behaviors of Pt, Re, and Os (Chabot et al., 2007).

Also recently, solid metal/liquid metal partitioning in the Fe–S system for P, V, Cr, Mn, Co, Ni, Cu, Zn, Ga, Sn, and Pb was reported by Stewart et al. (2009), who did not find any significant partitioning differences between their 9 to 23 GPa experiments. The main focus of their study was not to compare their results at elevated pressure to existing 0.1 MPa datasets but rather to introduce a modified lattice strain model for understanding the solid metal/liquid metal partitioning behaviors of trace elements. The lattice strain model has good success at fitting the characteristic parabolic trends present in their data, suggesting that the solid metal has an effect on the partitioning behavior of elements in this system. This demonstration of the effect of the solid metal on the partition coefficients provides a new perspective for understanding the behavior of elements in the Fe–S system, where 0.1 MPa studies have focused on the effect of the metallic liquid composition on the partitioning behavior.

Thus, previous studies have presented some intriguing and at times contradictory results, suggesting both that pressure may or may not affect solid metal/liquid metal partitioning behavior and that any effect may be highly dependent on the specific trace element. One of the complications in interpreting the existing datasets in terms of any pressure effect is that some of the datasets vary both pressure and S-content of the liquid, as well as the diversity of trace elements examined between the studies. For this work, we have conducted a series of experiments all at 9 GPa over a wide range of metallic liquid S compositions with numerous trace elements. This systematic dataset allows a direct comparison to the extensive 0.1 MPa data, enabling a clear examination of effects due to pressure as well as an examination of the proposed modified lattice strain model to rationalize the partitioning data.

2. Methods

All experiments were conducted at the University of New Mexico in a multi-anvil press at a pressure of 9 GPa. Experimental procedures were similar to those detailed in Chabot et al. (2008), who conducted solid metal–liquid metal experiments in the Fe–C system at 5 GPa. Tungsten–carbide cubes, with a truncated edge length of 8 mm, were used along with castable octahedral assemblies, as described in Agee et al. (1995). A Re foil furnace was used to heat the experiments, and the run temperature was monitored with a $W_{97}Re_3/W_{75}Re_{25}$ thermocouple placed perpendicular to the cylindrical Re foil furnace.

Starting powders of Fe and FeS were mixed with a few hundred ppms each of the trace elements Co, Ni, Cu, Ga, Ge, As, Mo, Ru, Rh, Pd, Ag, Sn, Sb, W, Re, Os, Ir, Pt, Au, Pb, and Bi. Powders were contained in alumina capsules. Run temperatures ranged from 1323 to 1873 K and run durations from 6 h to 30 min. The choice of starting bulk S contents and corresponding run temperatures were guided by the Fe–FeS phase diagram at 10 GPa of Chen et al. (2008) and selected to produce runs with about one-third solid metal and two-thirds liquid metal. At our experimental conditions of 9 GPa and a temperature range of 1323 to 1873 K, the solid Fe metal has a face-centered cubic (γ) structure (Boehler, 1986). To end the experiment, power to the Re foil furnace was turned off, quickly quenching the run at an isobaric condition. Run products were then extracted from the castable octahedra, mounted in epoxy, and cut and polished in preparation for analysis.

Experiments were first inspected and analyzed using the JEOL 8900L electron microprobe at the Carnegie Institution of Washington. Fig. 1 shows back-scattered electron images of a typical run product. In all of our experiments, the solid metal and liquid metal showed clear separation of the two phases, as seen in Fig. 1, enabling straightforward analysis of the chemical composition of each phase. The solid metal is preserved as a homogenous phase in the run product, but the metallic liquid quenched to a texture of Fe dendrites surrounded by interstitial FeS. The major elements of Fe and S were analyzed using the electron microprobe with beam conditions of 15 kV and 30 nA, a beam raster size of 10 μm × 10 μm, and a counting time of 30 s. For each solid or liquid phase, 15–20 microprobe measurements were averaged to determine the bulk composition, and errors were calculated as twice the standard error of the mean.

Trace element concentrations were measured by laser ablation inductively coupled plasma mass spectrometry (ICP-MS) at the University of Maryland, using techniques similar to those described in Chabot et al. (2008). *In situ* analyses were conducted using a single-collector ICP-MS (Element 2, Thermo Finnigan) coupled to a UV laser ablation system with an output wavelength at 213 nm (UP213, New Wave Research). The laser was operated with a uniform energy density of ~2–3 J/cm^2. Ablation sampling was conducted in line scan mode, with line lengths of ~100–500 μm, a 40-μm diameter spot size, and a 7 Hz flash rate. During analyses, the sample was moved at a rate of 10 μm/s. Four line scans were conducted in each solid metal and liquid metal phase. Data were collected for the following masses: ^{57}Fe, ^{59}Co, ^{62}Ni, ^{63}Cu, ^{65}Cu, ^{69}Ga, ^{71}Ga, ^{73}Ge, ^{75}As, ^{95}Mo, ^{97}Mo, ^{99}Ru, ^{101}Ru, ^{103}Rh, ^{105}Pd, ^{107}Ag, ^{108}Pd, ^{109}Ag, ^{117}Sn, ^{118}Sn, ^{121}Sb, ^{123}Sb, ^{182}W, ^{183}W,

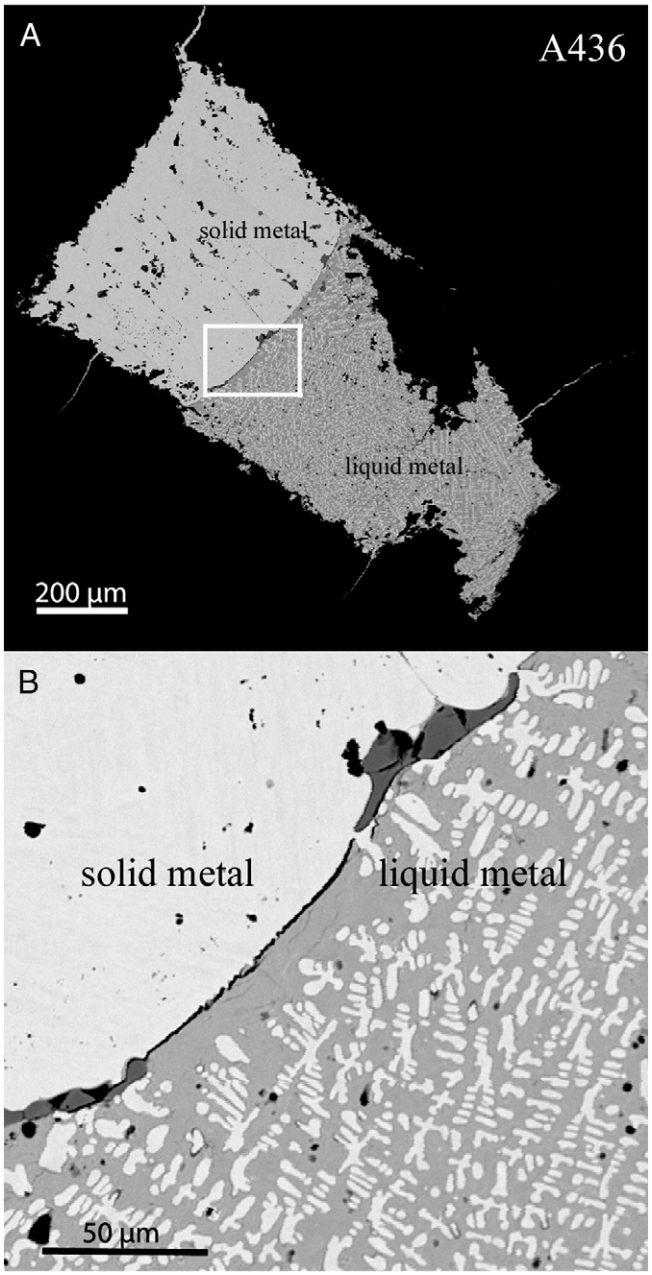

Fig. 1. Back-scattered electron images of run #A436, showing the two phases present in the experimental run products: Fe solid metal and S-bearing metallic liquid with a dendritic quench texture.

^{185}Re, ^{188}Os, ^{189}Os, ^{191}Ir, ^{193}Ir, ^{194}Pt, ^{195}Pt, ^{197}Au, ^{206}Pb, ^{208}Pb, and ^{209}Bi. When multiple isotopes were measured for a single element, the results were checked for consistency and the one with the higher signal was used. Analyses of two standard reference materials, North Chile (Filomena) (electronic annex of Walker et al., 2008) and NIST 610 (Jochum and Stoll, 2008) were conducted both before and after the analyses of the experimental run products and served as the basis for determining calibration curves to constrain instrument drift and provide element concentrations. Data were processed using the LAMTRACE software package (Achterbergh et al., 2001), which determines element concentrations using ratios of count rates for sample and standards, known concentrations in the standards, and the known concentration of an internal standard in the experimental run products, in this case Fe. The errors in the trace element concentrations were calculated as twice the standard error of the mean. Table 1 lists the concentrations measured for each of the run products, along with experimental details for each run.

At 5 GPa and 1523 K in the Fe–C system, Chabot et al. (2008) conducted a time series of solid metal/liquid metal partitioning experiments and showed that repeatable equilibrium partitioning was achieved for all 17 trace elements studied in less than 30 min. In our similar solid metal/liquid metal partitioning study here, we employed run durations of 30 min and greater, and four out of our seven runs were at temperatures >1523 K. Run #A434 was conducted at 1473 K and used a duration of 2 h to ensure equilibrium. The run product geometries of #A434 (1473 K), #A436 (1573 K), and #A435 (1773 K) allowed laser ablation ICP-MS line scans to be oriented perpendicular to the solid metal–liquid metal interface, enabling an examination for compositional gradients within the solid metal. No such gradients were seen in these three samples.

Two duplicate runs were conducted at our lowest temperature of 1323 K, one for 2 h (#A439) and another for 6 h (#A437). The measured partitioning results between these two duplicate experiments are in agreement within twice the standard error of the mean values reported in Table 1 for 14 of the 18 trace elements measured for both runs. The partitioning results for Co, Ru, and Rh agree within three standard errors of the mean, and W within four standard errors of the mean. Thus, because of this agreement, we chose to report values for both runs and not just the run with the longer duration. However, we note that the shorter run, #A439, produces some partitioning values that deviate slightly from the other data on the figures presented in the next section, and we consider that the shorter run duration potentially may be a contributing factor.

3. Results

Results are expressed as solid metal/liquid metal partition coefficients (D), which are listed in Table 1 and calculated as:

$$D(E) = \frac{\text{wt\%}E_{\text{solid metal}}}{\text{wt\%}E_{\text{liquid metal}}}. \quad (1)$$

One of the strengths of our new experimental results is the large number of elements for which partitioning data were obtained. This enables the data to be examined for trends consistent with an element's position in the periodic table. Figs. 2 and 3 compile all the data for the measured partitioning behavior of the 21 trace elements in our study and arrange the results in the order of the periodic table. Our new 9 GPa results are plotted in comparison to 0.1 MPa data. Data from other solid metal/liquid metal studies at elevated pressures in the Fe–S systems are also plotted in Figs. 2 and 3. Table E1 in the Electronic Supplement details the data sources for the 0.1 MPa and elevated pressure data shown in Figs. 2 and 3 and the fits to the 0.1 MPa data are tabulated in Chabot et al. (2010).

A basic observation can be made from inspection of Figs. 2 and 3, which is that our 9 GPa data differ noticeably from the 0.1 MPa data for the majority of the elements. Thus, different partitioning behaviors are observed as a function of the S content of the liquid for different pressures; pressure is affecting the partitioning behavior in this system.

However, Figs. 2 and 3 also demonstrate that the effect of pressure is different for different elements. For example, at 0.1 MPa, D(Mo) increases with increasing S-content of the metallic liquid, but at 9 GPa, Mo shows drastically different partitioning behaviors, with a slight decrease in D(Mo) with increasing S-content of the liquid. Our new 9 GPa data agree well with Lazar et al.'s (2004) 6 GPa data and Walker and Li's (2008) 2 to 4 GPa data, as shown in Fig. 2. Our new dataset shows that Mo is not the only element that changes its partitioning behavior significantly over this pressure range.

Moving from Mo across the fifth period elements in Figs. 2 and 3 to the other end of the periodic table, D(Sb) shows significant

Table 1
Conditions and results for 9 GPa solid metal/liquid metal experiments in the Fe–S system.

Run#	A433	A435	A432	A436	A434	A439	A437
T (K)	1873	1773	1673	1573	1473	1323	1323
Duration (min)	30	30	61	65	120	120	360
Liquid metal							
Fe (wt.%)	93.6 ± 0.8	91.2 ± 0.8	87.0 ± 0.5	83.0 ± 1.0	79.5 ± 0.9	77.8 ± 0.5	74.4 ± 0.6
S (wt.%)	5.2 ± 0.8	7.4 ± 0.8	11.4 ± 0.5	15.8 ± 0.9	18.8 ± 0.9	20.7 ± 0.5	22.5 ± 0.4
Co (ppm)	104 ± 7	97 ± 3	159 ± 3	121 ± 4	117 ± 4	74 ± 4	113 ± 9
Ni (ppm)	250 ± 130	660 ± 20	176 ± 11	290 ± 30	154 ± 10	300 ± 30	210 ± 40
Cu (ppm)	150 ± 20	203 ± 10	183 ± 8	190 ± 20	530 ± 60	260 ± 50	390 ± 70
Ga (ppm)	54 ± 6	49 ± 10	22 ± 3	20 ± 6	12 ± 2	11 ± 2	10 ± 2
Ge (ppm)	82 ± 5	100 ± 20	35 ± 3	25 ± 4	19 ± 3	29 ± 3	27 ± 2
As (ppm)	116 ± 9	125 ± 11	104 ± 10	91 ± 9	72 ± 2	80 ± 6	67 ± 7
Mo (ppm)	220 ± 20	260 ± 20	270 ± 20	230 ± 50	210 ± 30	173 ± 12	240 ± 60
Ru (ppm)	101 ± 5	66 ± 7	57 ± 4	31 ± 3	21 ± 2	26 ± 2	31 ± 2
Rh (ppm)	76 ± 3	47 ± 3	57 ± 8	20 ± 2	28 ± 2	31 ± 1	42 ± 4
Pd (ppm)	106 ± 6	108 ± 12	163 ± 13	94 ± 10	115 ± 10	98 ± 11	110 ± 30
Ag (ppm)	210 ± 60	320 ± 20	400 ± 60	230 ± 20	230 ± 30	190 ± 40	180 ± 50
Sn (ppm)	12 ± 4	13 ± 2	22 ± 4	570 ± 50	20 ± 3	28 ± 3	88 ± 8
Sb (ppm)	97 ± 3	330 ± 30	310 ± 20	81 ± 11	310 ± 30	230 ± 30	128 ± 12
W (ppm)	59 ± 6	62 ± 8	56 ± 3	33 ± 4	32 ± 3	66 ± 5	35 ± 1
Re (ppm)	80 ± 7	63 ± 8	43 ± 8	16 ± 3	19 ± 1	12 ± 4	12 ± 1
Os (ppm)	91 ± 5	32 ± 6	17 ± 2	8 ± 1	4.9 ± 0.3	4.2 ± 0.4	6 ± 2
Ir (ppm)	116 ± 6	44 ± 7	46 ± 5	18 ± 4	6.4 ± 0.4	5 ± 1	8 ± 1
Pt (ppm)	77 ± 6	54 ± 7	36 ± 4	21 ± 2	15 ± 1	16 ± 1	15 ± 2
Au (ppm)	160 ± 20	120 ± 12	171 ± 9	108 ± 12	88 ± 8	163 ± 9	100 ± 8
Pb (ppm)	160 ± 30	260 ± 20	800 ± 100	150 ± 30	240 ± 40	200 ± 40	178 ± 14
Bi (ppm)	200 ± 50	201 ± 12	390 ± 50	100 ± 20	140 ± 30	80 ± 20	380 ± 40
Solid metal							
Fe (wt.%)	99.1 ± 0.2	98.6 ± 0.3	98.8 ± 0.1	99.3 ± 0.2	98.7 ± 0.1	98.6 ± 0.2	99.0 ± 0.2
Co (ppm)	139 ± 13	115 ± 7	250 ± 100	162 ± 11	166 ± 12	74 ± 1	160 ± 30
Ni (ppm)	–	560 ± 60	180 ± 30	270 ± 20	138 ± 7	180 ± 20	180 ± 50
Cu (ppm)	114 ± 14	123 ± 6	90 ± 20	87 ± 9	270 ± 50	76 ± 8	170 ± 20
Ga (ppm)	83 ± 7	102 ± 3	75 ± 3	109 ± 9	100 ± 20	93 ± 2	110 ± 10
Ge (ppm)	110 ± 20	160 ± 20	110 ± 40	140 ± 30	150 ± 20	190 ± 60	210 ± 70
As (ppm)	70 ± 30	81 ± 10	100 ± 20	100 ± 9	120 ± 20	116 ± 7	140 ± 20
Mo (ppm)	120 ± 30	102 ± 8	100 ± 20	90 ± 12	80 ± 8	33 ± 8	74 ± 13
Ru (ppm)	169 ± 12	160 ± 20	200 ± 60	180 ± 30	150 ± 30	120 ± 30	290 ± 60
Rh (ppm)	91 ± 5	57 ± 12	150 ± 30	80 ± 20	110 ± 50	69 ± 10	160 ± 40
Pd (ppm)	62 ± 14	55 ± 11	81 ± 13	44 ± 7	50 ± 6	27 ± 3	39 ± 9
Ag (ppm)	22 ± 7	26 ± 6	25 ± 3	7 ± 2	5.4 ± 0.3	1.1 ± 0.2	1.6 ± 0.5
Sn (ppm)	–	–	4.8 ± 0.2	140 ± 30	8 ± 3	7 ± 1	25 ± 5
Sb (ppm)	29 ± 13	71 ± 5	93 ± 4	20 ± 3	101 ± 5	63 ± 2	46 ± 11
W (ppm)	69 ± 4	80 ± 5	100 ± 20	102 ± 9	102 ± 2	145 ± 10	120 ± 20
Re (ppm)	120 ± 80	146 ± 10	330 ± 110	150 ± 20	150 ± 30	200 ± 100	210 ± 100
Os (ppm)	240 ± 170	120 ± 30	170 ± 90	150 ± 40	160 ± 60	160 ± 106	–
Ir (ppm)	248 ± 11	160 ± 30	–	220 ± 50	120 ± 50	190 ± 60	230 ± 30
Pt (ppm)	128 ± 4	116 ± 14	150 ± 20	148 ± 11	145 ± 13	130 ± 40	220 ± 80
Au (ppm)	90 ± 30	56 ± 8	87 ± 7	66 ± 7	65 ± 4	84 ± 13	81 ± 14
Pb (ppm)	–	5 ± 2	10 ± 3	1.3 ± 0.3	1.6 ± 0.5	0.43 ± 0.04	–
Bi (ppm)	–	2.2 ± 1.0	2.3 ± 1.1	0.3 ± 0.2	0.5 ± 0.2	–	–
Partition coefficients							
Fe	1.06 ± 0.02	1.08 ± 0.02	1.14 ± 0.01	1.20 ± 0.02	1.24 ± 0.02	1.27 ± 0.01	1.33 ± 0.02
Co	1.3 ± 0.1	1.2 ± 0.1	1.6 ± 0.6	1.3 ± 0.1	1.4 ± 0.1	1.0 ± 0.1	1.5 ± 0.3
Ni	–	0.9 ± 0.1	1.0 ± 0.2	0.9 ± 0.1	0.9 ± 0.1	0.6 ± 0.1	0.8 ± 0.3
Cu	0.77 ± 0.13	0.60 ± 0.04	0.5 ± 0.1	0.45 ± 0.06	0.51 ± 0.11	0.3 ± 0.1	0.4 ± 0.1
Ga	1.5 ± 0.2	2.1 ± 0.4	3.4 ± 0.5	5 ± 2	8 ± 2	8 ± 2	11 ± 3
Ge	1.3 ± 0.2	1.7 ± 0.4	3.0 ± 1.1	5.6 ± 1.4	8 ± 2	7 ± 2	8 ± 3
As	0.6 ± 0.2	0.6 ± 0.1	0.9 ± 0.2	1.1 ± 0.2	1.6 ± 0.3	1.5 ± 0.1	2.0 ± 0.6
Mo	0.6 ± 0.1	0.39 ± 0.04	0.4 ± 0.1	0.4 ± 0.1	0.4 ± 0.1	0.19 ± 0.05	0.3 ± 0.1
Ru	1.7 ± 0.1	2.4 ± 0.4	4 ± 1	5.9 ± 1.2	7 ± 2	4.6 ± 1.1	9 ± 2
Rh	1.2 ± 0.1	1.2 ± 0.3	2.6 ± 0.6	3.8 ± 0.9	4 ± 2	2.2 ± 0.3	3.9 ± 0.9
Pd	0.6 ± 0.1	0.5 ± 0.1	0.5 ± 0.1	0.5 ± 0.1	0.4 ± 0.1	0.28 ± 0.04	0.4 ± 0.1
Ag	0.11 ± 0.05	0.08 ± 0.02	0.06 ± 0.01	0.03 ± 0.01	0.024 ± 0.004	0.006 ± 0.002	0.009 ± 0.005
Sn	–	–	0.22 ± 0.04	0.25 ± 0.06	0.4 ± 0.2	0.26 ± 0.05	0.3 ± 0.1
Sb	0.3 ± 0.1	0.22 ± 0.03	0.30 ± 0.02	0.25 ± 0.05	0.32 ± 0.03	0.28 ± 0.04	0.4 ± 0.2
W	1.2 ± 0.1	1.3 ± 0.2	1.7 ± 0.3	3.1 ± 0.4	3.2 ± 0.3	2.2 ± 0.2	3.5 ± 0.5
Re	1.4 ± 1.0	2.3 ± 0.4	8 ± 3	9 ± 2	7.8 ± 1.4	15 ± 10	18 ± 10
Os	3 ± 2	3.8 ± 1.1	10 ± 5	16 ± 5	31 ± 13	40 ± 30	–
Ir	2.1 ± 0.1	3.8 ± 0.9	–	12 ± 4	20 ± 7	37 ± 12	30 ± 5
Pt	1.7 ± 0.1	2.1 ± 0.4	4.1 ± 0.7	7.0 ± 1.0	9.6 ± 0.9	8 ± 3	14 ± 6
Au	0.5 ± 0.2	0.5 ± 0.1	0.51 ± 0.05	0.6 ± 0.1	0.7 ± 0.1	0.5 ± 0.1	0.8 ± 0.2
Pb	–	0.019 ± 0.007	0.014 ± 0.005	0.010 ± 0.006	0.007 ± 0.003	0.0021 ± 0.0005	–
Bi	–	0.011 ± 0.005	0.006 ± 0.003	0.003 ± 0.002	0.003 ± 0.002	–	–

All errors are ±2σ.
– = Measurement value <4σ and consequently not reported.

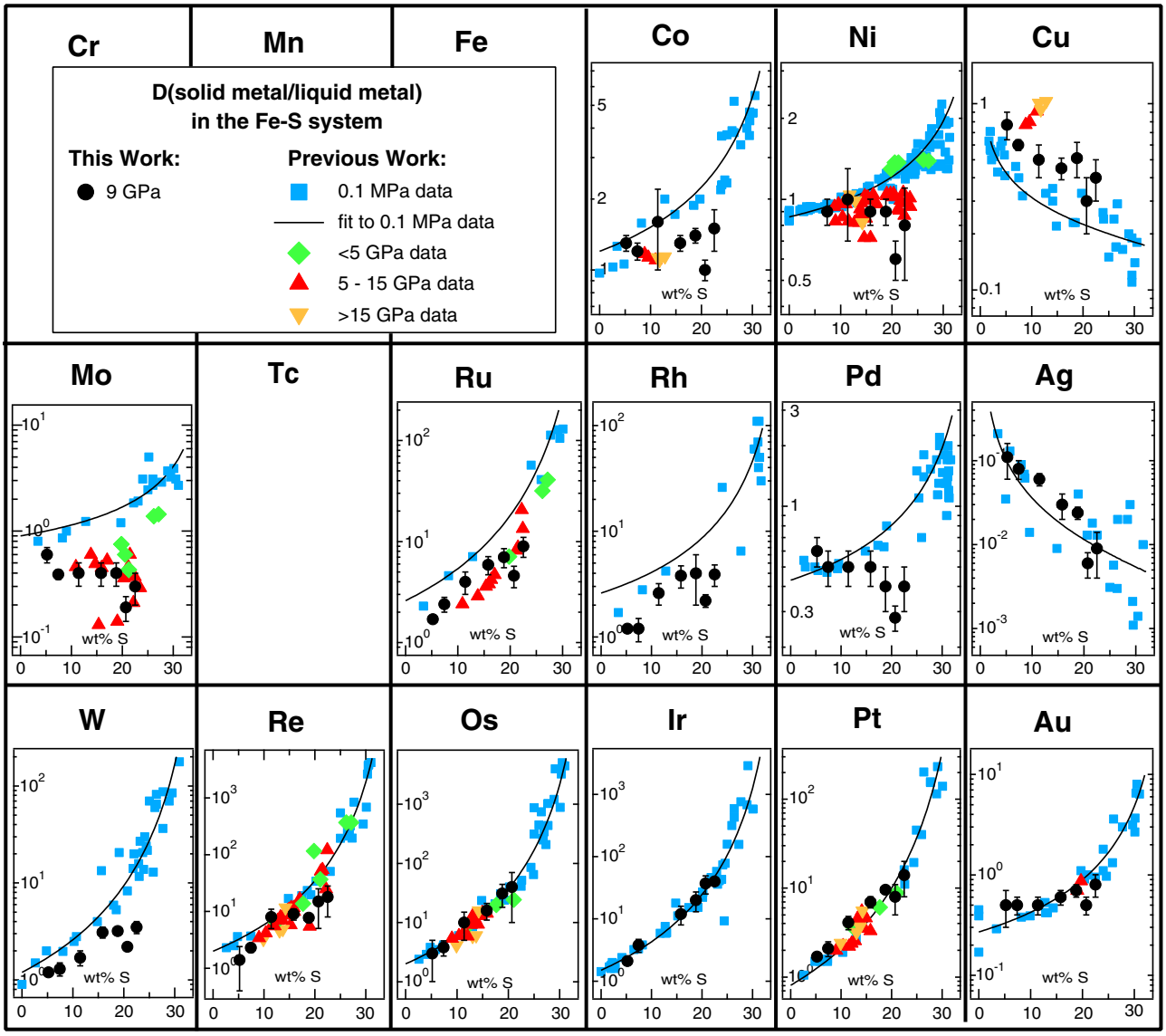

Fig. 2. Solid metal/liquid metal partitioning results in the Fe–S system. Elements are arranged according to their positions in the periodic table.

differences between the 0.1 MPa and 9 GPa datasets. In contrast to Mo, D(Sb) at 9 GPa is higher than at 0.1 MPa for a given S-content of the metallic liquid. In fact, all of the elements toward the right side of the periodic table (Ga, Ge, As, Sn, Sb, Pb, and Bi) show elevated D values at 9 GPa in comparison to their 0.1 MPa values, while elements toward the left of the periodic table (Mo, W, Ru, and Rh) have lower D values at 9 GPa than at 0.1 MPa.

Many of the elements that show the greatest change in their partitioning behaviors as a function of the S-content of the metallic liquid, show little to no change in their behavior between 0.1 MPa and 9 GPa. For the highly siderophile elements of Re, Os, Ir, and Pt, our new 9 GPa data fall within error of the 0.1 MPa data, as shown in Fig. 2.

In addition to some D values being higher, some lower, and some the same at 9 GPa compared with 0.1 MPa, the partitioning behavior for many elements at 9 GPa appears to have a different dependency on the S-content of the liquid than at 0.1 MPa. Based on 0.1 MPa data, Jones and Malvin (1990) suggested that the solid metal/liquid metal partitioning behaviors of elements in the Fe–S system were controlled by S avoidance in the metallic liquid and that the metallic liquid could be envisioned as being composed of Fe and FeS domains. As the S content of the metallic liquid increased, the availability of Fe domains in the liquid decreased, and siderophile elements partitioned more strongly in the solid metal phase. When plotted as a function of the S-content of the metallic liquid, the D values for such elements increased with increasing S content and the increase became more extreme at higher S contents. Chabot and Jones (2003) modified the mathematical representation of this general concept slightly, leading to the 0.1 MPa fitted curves shown in Figs. 2 and 3.

In contrast to the 0.1 MPa curves, at 9 GPa, many elements show less overall change in their D values with changing S conditions. For example, D(Ni) maintains a near constant value over the range of S-contents examined at 9 GPa, in contrast to the 0.1 MPa behavior. Other experimental studies at elevated pressures also show this change in D(Ni) from 0.1 MPa values, though the previous studies did not comment on the difference. Other elements that also suggest a flattening of their dependence on the S content of the metallic liquid at 9 GPa include Co, Pd, Sn, Sb, and Au. This change in the dependency on the S content of the metallic liquid suggests that the controlling factor at 9 GPa on the partitioning behavior has changed from the 0.1 MPa theory based on Fe domains in the liquid. Such a change has implications for applying any partitioning data in the Fe–S system from one pressure to another. Recent work suggests that the structure of Fe–FeS melts may undergo an important transition near ~15 GPa (Morard et al., 2007). If the liquid structure is beginning to evolve in

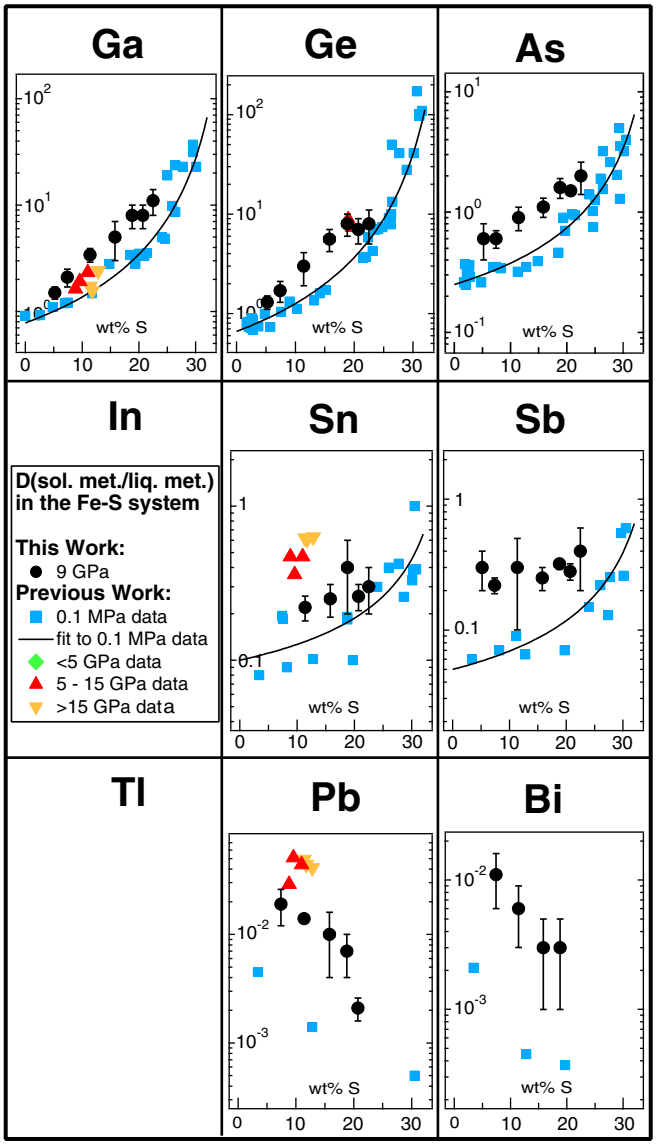

Fig. 3. Solid metal/liquid metal partitioning results in the Fe–S system. Elements are arranged according to their positions in the periodic table.

our runs, it could explain some of the pressure effects we note in our partitioning data.

Though we currently do not understand many of the differences we have noted between our 9 GPa data and 0.1 MPa values, our data clearly show that pressure is affecting the partitioning behavior in this system. In the next section, we apply our new data to a recently published lattice strain model and discuss planetary implications of the effects of pressure observed in our data.

4. Discussion

4.1. Application to a lattice strain model

Using 0.1 MPa data, a parameterization method for solid metal/liquid metal partitioning data in the Fe–S system was developed based on the general theory that the S content of the metallic liquid, not the temperature or the solid metal, was the dominant influence on the partitioning behavior (Chabot and Jones, 2003; Jones and Malvin, 1990). Recently, Stewart et al. (2009) applied a lattice strain model to Fe–S data, mainly at elevated pressures, and suggested that the solid metal plays an important role in governing the solid metal/liquid metal partitioning behavior of trace elements. Here we use our new 9 GPa dataset to examine the proposed lattice strain parameterization method of Stewart et al. (2009).

The main lattice strain model equation presented in Stewart et al. (2009) for metallic systems is:

$$D_i = D_o(T,P)^* \exp\left[\left(-4\pi N_A E\left[\frac{1}{2} r_o (r_i - r_o)^2 + \frac{1}{3}(r_i - r_o)^3\right]\right) / RT\right]. \quad (2)$$

Where D_i and r_i are the partition coefficient and the radius respectively of the neutral atom i that is incorporated into the solid metal crystal structure site with an ideal partition coefficient of $D_o(T, P)$, for the relevant temperature and pressure, and ideal radius of r_o. The quantity E is the apparent Young's modulus for the site, N_A is Avogadro's number, R is the gas constant, and T is the temperature. In the Stewart et al. (2009) model, r_i is the neutral atom radius for each element calculated by Clementi et al. (1967).

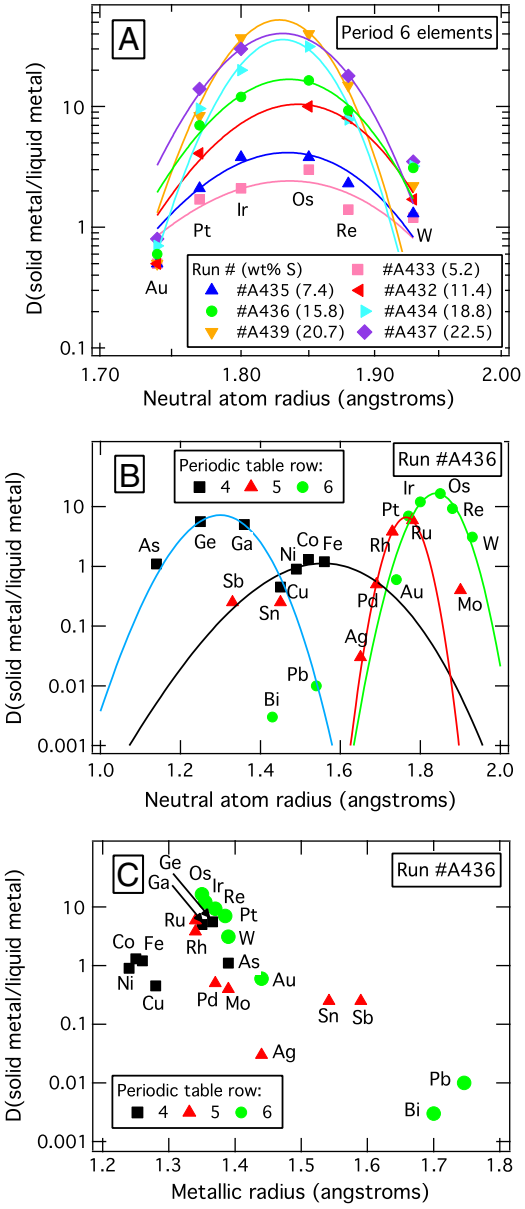

Fig. 4. The lattice strain model of Stewart et al. (2009) applied to A) sixth period elements in all of our runs and B) all elements measured in run #A436. C) The same element data measured in run #A436 are plotted against metallic radius.

In their study, Stewart et al. (2009) first applied this parameterization model to six experiments in the Fe–S system at pressures between 9 and 23 GPa for elements in the fourth row of the periodic table: V, Cr, Mn, Fe, Co, and Ni. At the experimental conditions of Stewart et al. (2009), the solid Fe metal had a face-centered cubic (γ) structure, just as the solid Fe metal in our runs (Boehler, 1986). They found that all six experiments were well-fit by the resulting parabolas centered on an ideal radius near the neutral atom size of Fe (1.56 Å, Clementi et al., 1967). Additionally, similar parabolic fits were found for the six experiments in their study, despite changes in the pressure and temperature of each run. Our data for fourth period elements are more limited than Stewart et al. (2009), but our D(Ni) and D(Co) data in Fig. 2 show that both of these elements are becoming insensitive to the composition of the metallic liquid, with near constant D values over a wide range of S-contents. This supports the finding of a single parabolic fit to explain these elements over a range of temperatures.

In Fig. 4A we apply the Stewart et al. (2009) lattice strain model to our 9 GPa data for six elements from the sixth row of the periodic table. Table 2 provides the D_o, r_o, and E values determined for each fit. Our data are nicely fit with the parabolas shown in Fig. 4A, and all seven of our experiments suggest a similar ideal radius r_o of about 1.83 Å, which is the same r_o determined by Stewart et al. (2009) for these elements. Stewart et al. (2009) suggested that this larger radius site may be related to a defect site in the crystal lattice.

In contrast to the findings of Stewart et al. (2009) for the fourth period elements, our data for the sixth period elements in Fig. 4A show significantly different parabolic fits for different experiments. The parabolic fits vary systematically with the S-content of the metallic liquid, which is directly related to the 1323–1873 K temperature range of the runs as well as metallic liquid compressibility (Sanloup et al., 2000). Also, as the S-content of the liquid increases and the temperature decreases, the fits become less able to match the two end-members (Au and W) in Fig. 4A. The Stewart et al. (2009) lattice strain model can match a given experiment for the sixth period elements, but such a model does not explain why our seven experiments all conducted at a pressure of 9 GPa require different parabolic fits. The metallic liquid composition, as seen in Fig. 2, can have a significant effect on the partition coefficients for sixth period elements, causing order of magnitude changes in the D values. Effects from the liquid metal composition or temperature beyond those included in the Stewart et al. (2009) lattice strain model appear to be significantly influencing partitioning in this system. van Westrenen et al. (2000) have demonstrated that the fitted lattice strain parameters can be influenced by properties of the melt in crystal/melt systems, and consideration of the metallic melt seems required by any parameterization model in the Fe–S system as well.

Stewart et al. (2009) suggested the presence of a third site, occupied by Cu, Zn, Ga, Sn, and Pb, elements with chalcophile tendencies. Consequently, we applied Eq. (2) to data for the elements Cu, Ga, Ge, As, Sn, and Pb, and the results are given in Table 2. Like the fits shown in Fig. 4A, the parameters of the fits and the resulting shapes of the parabolas varied regularly as the S content of the liquid increased and the temperature decreased. Additionally, we applied Eq. (2) to the fifth period elements of Mo, Ru, Rh, Pd, and Ag. These fifth period elements were also fairly well-fit by the resulting parabolas, but the fitted parameters given in Table 2 again varied regularly with the S-content of the metallic liquid and run temperature.

In Fig. 4B we plot all of the D values measured in run #A436. Run #A436 lies in the middle of the temperature range and liquid S content for the experiments in this study, and D values were determined for all trace elements in this run, making it a good choice for inspection in Fig. 4B. In Fig. 4B, the best fit for the sixth period elements from Fig. 4A is included, as are parabolic fits for period 5 elements Mo, Ru, Rh, Pd, and Ag and for elements with chalcophile tendencies (Cu, Ga, Ge, As, Sn, and Pb). Since the Stewart et al. (2009) data for fourth period elements are more extensive than ours, we used a fit determined in that study from an experiment at 9 GPa and 1523 K; the fit is consistent with the D(Ni), D(Co), and D(Fe) values measured in run #A436 and shown in Fig. 4B and listed in Table 2.

With the four parabolic fits in Fig. 4B, only Bi is not generally matched. The success of being able to fit 21 elements with four sites with the crystal lattice model is noteworthy. However, the size of the radius alone doesn't appear to be the only control on the behavior of the elements. For example, Sb has a radius intermediate to Ge and Ga, yet it is not falling on the same parabolic fit as these two elements. Similarly, Pb has a radius very near that of Fe, but D(Pb) is not consistent with partitioning into the site centered on Fe.

Additionally, a complication to the application of a lattice strain model to this system is the choice of appropriate atomic radii in the model. Following the approach used by Stewart et al. (2009), Fig. 4A and B use the neutral atomic radii calculated by Clementi et al. (1967). However, the Clementi et al. (1967) values differ significantly from metallic radii (Pauling, 1947, 1949; Greenwood and Earnshaw, 1997). Fig. 4C shows the same data from run #A436 as Fig. 4B but plotted against metallic radii, and the characteristic parabolic trends of the lattice strain model no longer appear in the dataset. In modeling Re, Os, and Pt in their study, Van Orman et al. (2008) chose to use the metallic radii, and we also feel that the choice of metallic radii seems more relevant to this system. The Clementi et al. (1967) radii may be most appropriate for gaseous neutral atoms and possibly are not appropriate for a solid metal where metallic bonding, extensive delocalization of electrons, and promotion of electrons into higher-energy orbitals (to promote bonding) all occur routinely.

Thus, the success of the parabolic fits in Fig. 4A and B is intriguing, but it seems necessary to include the significant effect of the metallic liquid composition in any parameterization expression for partitioning in the Fe–S system. Additionally, the lattice strain model does not use the metallic radii values, which we feel are most appropriate to the Fe–S system.

4.2. Partitioning of Pt, Re, and Os

Elevated $^{186}Os/^{188}Os$ and $^{187}Os/^{188}Os$ ratios in mantle plume sources led to the suggestion that the distinctive Os isotopic signature was being imparted by Earth's core (Brandon and Walker, 2005;

Table 2
Fitted parameterization values.

Run #	S (wt.%)	T (K)	Elements fit	D_o	r_o (Å)	E (GPa)
A433	5.2	1873	W, Re, Os, Ir, Pt, Au	2.4	1.84	266
A435	7.4	1773		4.2	1.83	360
A432	11.4	1673		10.4	1.84	333
A436	15.8	1573		16.8	1.84	463
A434	18.8	1473		35.9	1.83	811
A439	20.7	1323		48.9	1.83	748
A437	22.5	1323		40.4	1.83	504
A433	5.2	1873	Cu, Ga, Ge, As, Sn, Pb	1.6	1.31	111
A435	7.4	1773		2.3	1.31	177
A432	11.4	1673		4.2	1.31	253
A436	15.8	1573		7.2	1.30	264
A434	18.8	1473		11.1	1.30	273
A439	20.7	1323		11.3	1.31	299
A437	22.5	1323		15.4	1.31	355
A433	5.2	1873	Mo, Ru, Rh, Pd, Ag	1.8	1.80	234
A435	7.4	1773		2.5	1.80	352
A432	11.4	1673		4.1	1.78	433
A436	15.8	1573		6.6	1.76	940
A434	18.8	1473		7.8	1.77	976
A439	20.7	1323		4.7	1.77	665
A437	22.5	1323		9.2	1.77	740
A436	15.8	1573	Fe, Co, Ni	1.12[a]	1.56[a]	81[a]

[a] Values from Stewart et al. (2009) fit of V, Cr, Mn, Fe, Co, and Ni for run #129 (9 GPa, 1523 K).

Brandon et al., 1998, 1999, 2003; Puchtel et al., 2005; Walker et al., 1995, 1997). ^{187}Re decays to ^{187}Os with a half-life of ~42 Ga years and ^{190}Pt decays to ^{186}Os with a half-life of ~489 Ga years. Thus, a source region with elevated ratios of ^{186}Os/^{188}Os and ^{187}Os/^{188}Os indicates that the source was enriched in Re and Pt relative to Os and, given the long half-lives in this system, such enrichment must have occurred prior to 2.5 Ga. Using iron meteorite and 0.1 MPa solid metal/liquid metal experimental data, Brandon et al. (1999) and Walker et al. (1995) proposed that the ongoing crystallization of Earth's solid inner core may have left the liquid outer core enriched in Pt and Re relative to Os and that the more radiogenic Os isotopic signature in the mantle plume source was due to exchange between the liquid outer core and the mantle. This hypothesis has been debated (Brandon and Walker, 2005), with discussions of the lack of a W isotopic anomaly (Schersten et al., 2004), the contributions of crustal recycling (e.g. Sobolev et al., 2008), and the timing of Earth's inner core formation (Lassiter, 2006). Our new 9 GPa data allow us to examine the effect of pressure on the solid metal/liquid metal partitioning behaviors of Pt, Re, and Os in the Fe–S system.

Fig. 5 shows all existing solid metal/liquid metal partitioning data for Pt, Re, and Os in the Fe–S system. Because of the interest in these specific elements, there are a number of elevated pressure data in addition to our new 9 GPa results. Overall, there is no change in D(Pt), D(Re), or D(Os) as a function of pressure, including data from 0.1 MPa to 22 GPa. In contrast, Van Orman et al. (2008) concluded that D(Pt), D(Re), and D(Os) all decreased with increasing pressure. The three highest pressure data points of Van Orman et al. (2008) do fall lower than the 0.1 MPa trend (Fig. 5B and C). However, the decrease is slight and well within the scatter of the overall experimental datasets. Also, the 20 GPa data of Hayashi et al. (2009) are entirely consistent with the 0.1 MPa data and do not support the conclusion of Van Orman et al. (2008) that pressure causes a decrease in the partition coefficients for these three elements.

Van Orman et al. (2008) proposed that the way in which pressure affected an element's D value was related to an element's compressibility relative to Fe. Since Pt, Re, and Os were much less compressible than Fe, increasing pressure resulted in an increasing misfit for these elements into the Fe substitution site and led to a decrease in their solid metal/liquid metal partition coefficient. Our 9 GPa dataset do reveal trends associated with moving across a row in the periodic table, and possibly this could be due to an element's compressibility. However, we see the least effect of pressure for elements that are not very compressible, such as Pt, Re, and Os.

Brandon et al. (2003) modeled the crystallization of Earth's inner core and the effects that different timings of formation of the inner core would have on the possible fractionations of Pt, Re, and Os. They identified a few different model scenarios, with values for D(Pt), D(Re), and D(Os), that could match the Os isotopic signature observed in mantle plume sources. These D values from Brandon et al. (2003) are plotted in Fig. 5 as horizontal green shaded regions. There are experimental determinations for D(Pt), D(Re), and D(Os) that fall in these green regions. However, another limitation that needs to be placed on the data is the range of S contents allowed in Earth's core; a maximum S-content of ~10% is allowed if S was the only light element in Earth's core, but S estimates for Earth's core based on cosmochemical arguments estimate a value closer to ~2% (e.g. McDonough, 2003). The range of allowed S contents for Earth's core is plotted as shaded yellow regions in Fig. 5. For Re and Os, the experimental data are far from overlapping with both the green and yellow shaded regions simultaneously. In many cases, the experimental data for D(Re) and D(Os) are about an order of magnitude too low to create the fractionations required to produce the Os isotopic signature measured in mantle plume sources.

Overall, our new 9 GPa data for D(Pt), D(Re), and D(Os) are consistent with most other elevated pressure studies and do not support an effect of pressure on the partitioning behavior of these elements over this pressure range. Over the pressure range studied, which extends up to 22 GPa, the observed values for D(Re) and D(Os) are too low to produce the fractionations required to explain the elevated ^{186}Os/^{188}Os and ^{187}Os/^{188}Os ratios from mantle plume sources with a S content appropriate for Earth's core. However, these experiments are all still done at considerably lower pressures than that of Earth's core and it is unknown if higher pressure will change the partitioning behavior of these elements.

4.3. Considerations for differentiation models

During differentiation, metal separates from silicate, and how elements partition between these two phases is known to be dependent on a number of variables, such as pressure, temperature, oxygen fugacity, silicate composition, and metal composition. Studies of planetary differentiation often use metal/silicate partitioning values determined experimentally over a variety of pressure and temperature conditions to model chemically the differentiation process. Our results here suggest that the effect of metal composition may be dependent on pressure and, if so, there may be important ramifications for differentiation models.

The two most common elements modeled during studies of Earth's core formation are Ni and Co, due to their moderately siderophile and refractory natures (Chabot et al., 2005; Gessmann and Rubie, 2000;

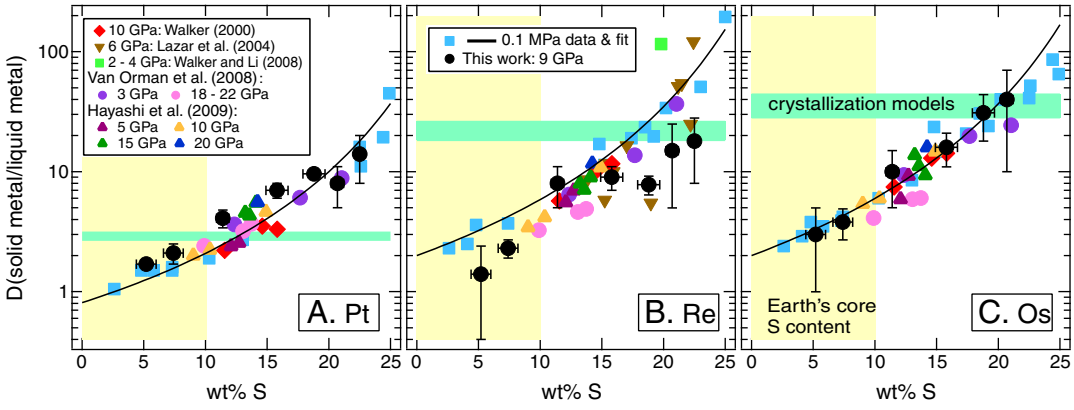

Fig. 5. Solid metal/liquid metal partitioning data in the Fe–S system for A) Pt, B) Re, and C) Os. The range of allowed S contents for Earth's core is shaded in yellow. The horizontal green shaded regions are the partitioning values required by Earth's inner core crystallization models of Brandon et al. (2003) to match the elevated ^{186}Os/^{188}Os and ^{187}Os/^{188}Os ratios measured in mantle plume sources. The intersection between the green shaded region and the data do not overlap with an upper limit (10 wt.%) for the S content of the core, and Earth's core may have substantially less S with only ~2 wt.%.

Kegler et al., 2008; Li and Agee, 1996, 2001; Righter and Drake, 1999; Righter et al., 1997; Wade and Wood, 2005; Wood et al., 2008). Numerous solid metal/liquid metal data from 0.1 MPa studies suggest that as the S content of the metallic liquid increases, both Ni and Co partition less into the liquid metal, displaying typical S avoidance tendencies, as seen in Fig. 2. But as also seen in Fig. 2, our data show a very different effect of S on the partitioning behavior of these elements at 9 GPa. At 9 GPa, over a large range of S contents, D(Ni) and D(Co) are nearly constant and insensitive to the S content of the metallic liquid. Thus, if one were combining 0.1 MPa metal/silicate data with 9 GPa metal/silicate data for Ni and Co in a differentiation model, the method to account for the effect of S would need to be different for the data from the two different pressures. Applying the effect of S determined at 0.1 MPa to the 9 GPa data would result in an incorrect predicted behavior, while assuming that the S content did not have an effect on the behavior would be incorrect for the 0.1 MPa data. Previous models of Earth's core formation have included metal/silicate determinations of Ni and Co over a range of pressures and used linear regressions, some with a non-pressure dependent metallic composition term, to model the data. Our results suggest that such models are likely not accounting for the effect of S accurately and even may be introducing flaws into their linear regression expressions.

Two other refractory, moderately siderophile elements important to differentiation models are Mo and W (Cottrell et al., 2009, 2010; Righter and Drake, 1999; Righter et al., 1997; Wade and Wood, 2005). As seen in Fig. 2, both of these elements exhibit different partitioning behaviors at 9 GPa than at 0.1 MPa. The change in D(Mo) is especially pronounced, changing from increasing with increasing S content of the metallic liquid 0.1 MPa to decreasing slightly with increasing S at 9 GPa. The effects of higher pressures on D(Mo) and D(W) are unknown. A differentiation model that utilizes S-bearing metal/silicate experiments over a range of pressures may need to take special care to properly deal with the effect of S on the partitioning behaviors of W and Mo given the pressure dependency suggested by our data.

For differentiation models, there are two main issues that need to be considered for properly including the effect of S in the model: 1) How to correctly combine and compare S-bearing experimental datasets conducted at different pressures. Experimental studies based on natural starting compositions often produce very S-rich metallic liquid compositions (e.g. Li and Agee, 1996, 2001), making the proper treatment of the effect of S even more important. 2) How to include a S term in the model expressions. Current differentiation models that include a term for the effect of S in the metallic composition do not have any pressure dependency in that S term (e.g. Righter et al., 1997). Our results suggest that the effect of S on partitioning behavior is influenced by pressure and thus trying to express the effect of S as the same over a range of pressures may produce inaccurate model results.

Further work is needed to better address these two main issues. Metal/silicate experiments designed to examine the effects of metallic composition over a range of pressures could be particularly insightful. Our solid metal/liquid metal results suggest that the effect of metallic composition is dependent on pressure, and this complication is not being addressed in current differentiation models.

5. Conclusions

For the Fe–S system, our 9 GPa solid metal/liquid partitioning results differ significantly from 0.1 MPa values for the majority of elements studied. For some elements, the effect of pressure appears to be more than just offsetting the D values to higher or lower values. Rather, the fundamental dependency of the partitioning behavior on the liquid S composition appears to be different for some elements from 0.1 MPa to 9 GPa. In contrast, for a few elements, we do not observe any significant change in their partitioning behavior from 0.1 MPa to 9 GPa. The power of such a large experimentally-derived dataset, with 21 trace elements and experiments that span 5–22 wt.% S and 1323–1873 K, is that it reveals trends consistent with the periodic table and provides predictive tools for future studies that seek to understand better how and why metallic composition influences partitioning behavior as a function of pressure.

Supplementary materials related to this article can be found online at doi: 10.1016/j.epsl.2011.03.027.

Acknowledgments

This work was supported by NASA Cosmochemistry grant NNX09AG90G to NLC, NASA Cosmochemistry grant NNX08AH76G, NSF grant no. 0739006 to WFM, and a NASA RTOP to JHJ. We thank W. van Westrenen, an anonymous reviewer, and R. W. Carlson for comments that led to an improved and clarified paper.

References

Achterbergh, E.V., Ryan, C.G., Jackson, S.E., Griffin, W.L., 2001. Appendix 3: data reduction software for LA-ICP-MS. In: Sylvester, P. (Ed.), Laser Ablation-ICP-MS in the Earth Sciences: Mineralogical Association of Canada, Short Course Series, vol. 29. 243 pp.

Agee, C.B., Li, J., Shannon, M.C., Circone, S., 1995. Pressure–temperature phase diagram for the Allende meteorite. J. Geophys. Res. 100, 17725–17740.

Boehler, R., 1986. The phase diagram of iron to 430 kbar. Geophys. Res. Lett. 13 (11), 1153–1156.

Brandon, A.D., Walker, R.J., 2005. The debate over core–mantle interaction. Earth Planet. Sci. Lett. 232, 211–225.

Brandon, A.D., Walker, R.J., Morgan, J.W., Norman, M.D., Prichard, H.M., 1998. Coupled ^{186}Os and ^{187}Os evidence for core–mantle interaction. Science 280, 1570–1573.

Brandon, A.D., Norman, M.D., Walker, R.J., Morgan, J.W., 1999. ^{186}Os–^{187}Os systematics of Hawaiian picrites. Earth Planet. Sci. Lett. 174, 25–42.

Brandon, A.D., Walker, R.J., Puchtel, I.S., Becker, H., Humayun, M., Revillon, S., 2003. ^{186}Os–^{187}Os systematics of Gorgona Island komatiites: implications for early growth of the inner core. Earth Planet. Sci. Lett. 206, 411–426.

Chabot, N.L., Haack, H., 2006. Evolution of asteroidal cores. In: Lauretta, D.S., McSween Jr., H.Y. (Eds.), Meteorites and the Early Solar System II. The University of Arizona Press, Tucson, pp. 747–771.

Chabot, N.L., Jones, J.H., 2003. The parameterization of solid metal–liquid metal partitioning of siderophile elements. Meteorit. Planet. Sci. 38, 1425–1436.

Chabot, N.L., Campbell, A.J., Jones, J.H., Humayun, M., Agee, C.B., 2003. An experimental test of Henry's Law in solid metal–liquid metal systems with implications for iron meteorites. Meteorit. Planet. Sci. 38, 181–196.

Chabot, N.L., Draper, D.S., Agee, C.B., 2005. Conditions of core formation in the Earth: constraints from nickel and cobalt partitioning. Geochim. Cosmochim. Acta 69, 2141–2151.

Chabot, N.L., Saslow, S.A., McDonough, W.F., McCoy, T.J., 2007. The effect of Ni on element partitioning during iron meteorite crystallization. Meteorit. Planet. Sci. 42, 1735–1750.

Chabot, N.L., Campbell, A.J., McDonough, W.F., Draper, D.S., Agee, C.B., Humayun, M., Watson, H.C., Cottrell, E., Saslow, S.A., 2008. The Fe–C system at 5 GPa and implications for Earth's core. Geochim. Cosmochim. Acta 72, 4146–4158.

Chabot, N.L., Saslow, S.A., McDonough, W.F., Jones, J.H., 2009. An investigation of the behavior of Cu and Cr during iron meteorite crystallization. Meteorit. Planet. Sci. 44, 505–519.

Chabot, N.L., Safko, T.M., McDonough, W.F., 2010. Effect of silicon on trace element partitioning in iron-bearing metallic melts. Meteorit. Planet. Sci. 45, 1243–1257.

Chen, B., Li, J., Hauck II, S.A., 2008. Non-ideal liquidus curve in the Fe–S system and Mercury's snowing core. Geophys. Res. Lett. 35. doi:10.1029/2008GL033311.

Clementi, E., Raimondi, D.L., Reinhardt, W.P., 1967. Atomic screening constants from SCF functions. II. Atoms with 37 to 86 electrons. J. Chem. Phys. 47, 1300–1307.

Cottrell, E., Walter, M.J., Walker, D., 2009. Metal-silicate partitioning of tungsten at high pressure and temperature: implications for equilibrium core formation in Earth. Earth Planet. Sci. Lett. 281, 275–287.

Cottrell, E., Walter, M.J., Walker, D., 2010. Erratum to "Metal-silicate partitioning of tungsten at high pressure and temperature: implications for equilibrium core formation in Earth.". Earth Planet. Sci. Lett. 289, 631–634.

Gessmann, C.K., Rubie, D.C., 2000. The origin of the depletions of V, Cr, and Mn in the mantles of the Earth and Moon. Earth Planet. Sci. Lett. 184, 95–107.

Greenwood, N.N., Earnshaw, A., 1997. Chemistry of the Elements, Second Edition. Butterworth-Heinemann, Oxford. 1600 pp.

Hayashi, H., Ohtani, E., Terasaki, H., Ito, Y., 2009. The partitioning of Pt–Re–Os between solid and liquid metal in the Fe–Ni–S system at high pressure: implications for inner core fractionation. Geochim. Cosmochim. Acta 73, 4836–4842.

Humayun, M., Keil, K., Bischoff, A., 2009. Siderophile elements in metal from Northwest Africa 2526, and enstatite chondrite partial melt residue. 40th Lunar and Planetary Science Conference, p. 1744.

Jochum, K.P., Stoll, B., 2008. Reference materials for elemental and isotopic analyses by LA-(MC)-ICP-MS: successes and outstanding needs. Chapter 10 In: Sylvester, P. (Ed.), Laser-Ablation-ICP-MS in the Earth Sciences: Current Practices and

Outstanding Issues: Mineralogical Association of Canada Short Course, vol. 40, pp. 147–168. Vancouver, B.C.
Jones, J.H., Malvin, D.J., 1990. A nonmetal interaction model for the segregation of trace metals during solidification of Fe–Ni–S, Fe–Ni–P, and Fe–Ni–S–P alloys. Metall. Trans. 21B, 697–706.
Jones, J.H., Walker, D., 1991. Partitioning of siderophile elements in the Fe–Ni–S system: 1 bar to 80 kbar. Earth Planet. Sci. Lett. 105, 127–133.
Kegler, Ph., Holzheid, A., Frost, D.J., Rubie, D.C., Dohmen, R., Plame, H., 2008. New Ni and Co metal-silicate partitioning data and their relevance for an early terrestrial magma ocean. Earth Planet. Sci. Lett. 268, 28–40.
Lassiter, J.C., 2006. Constraints on the coupled thermal evolution of the Earth's core and mantle, the age of the inner core, and the origin of the $^{186}Os/^{188}Os$ "core signal" in plume-derived lavas. Earth Planet. Sci. Lett. 250, 306–317.
Lazar, C., Walker, D., Walker, R.J., 2004. Experimental partitioning of Tc, Mo, Ru, and Re between solid and liquid during crystallization in Fe–Ni–S. Geochim. Cosmochim. Acta 68, 643–651.
Li, J., Agee, C.B., 1996. Geochemistry of mantle–core differentiation at high pressure. Nature 381, 686–689.
Li, J., Agee, C.B., 2001. The effect of pressure, temperature, oxygen fugacity and composition on partitioning of nickel and cobalt between liquid Fe–Ni–S alloy and liquid silicate: implications for the Earth's core formation. Geochim. Cosmochim. Acta 65, 1821–1832.
McDonough, W.F., 2003. Compositional models for the Earth's core. In: Carlson, R.W. (Ed.), The Mantle and Core. In: Holland, H.D., Turekian, K.K. (Eds.), Treastise on Geochemistry, vol. 2. Elsevier-Pergamon, Oxford, pp. 547–568.
Morard, G., Sanloup, C., Fiquet, G., Mezouar, M., Rey, N., Poloni, R., Beck, P., 2007. Structure of eutectic Fe–FeS melts to pressures up to 17 GPa: implications for planetary cores. Earth Planet. Sci. Lett. 263, 128–139.
Pauling, L., 1949. A resonating-valence-bond theory of metals and intermetallic compounds. Proc. R. Soc. London Ser. A 196 (1046), 343–362.
Pauling, L., 1947. Atomic radii and interatomic distances in metals. J. Am. Chem. Soc. 69, 542–553.
Puchtel, I.S., Brandon, A.D., Humayun, M., Walker, R.J., 2005. Evidence for the early differentiation of the core from Pt–Re–Os isotope systematics of 2.8 Ga komatiites. Earth Planet. Sci. Lett. 237, 118–134.
Rankenburg, K., Humayun, M., Brandon, A.D., Herrin, J.S., 2008. Highly siderophile elements in ureilites. Geochim. Cosmochim. Acta 72, 4642–4659.
Righter, K., Drake, M.J., 1999. Effect of water on metal-silicate partitioning of siderophile elements: a high pressure and temperature terrestrial magma ocean and core formation. Earth Planet. Sci. Lett. 171, 383–399.
Righter, K., Drake, M.J., Yaxley, G., 1997. Prediction of siderophile element metal/silicate partition coefficients to 20 GPa and 2800 °C: the effects of pressure, temperature, oxygen fugacity and silicate and metallic melt compositions. Phys. Earth Planet. Int. 100, 115–134.
Sanloup, C., Guyot, F., Gillet, P., Fiquet, G., Mezouar, M., Martinez, I., 2000. Density measurements of liquid Fe–S alloys at high pressure. Geophys. Res. Lett. 27, 811–814.
Schersten, A., Elliott, T., Hawkesworth, C., Norman, M., 2004. Tungsten isotope evidence that mantle plumes contain no contribution from the Earth's core. Nature 427, 234–237.
Sobolev, A.V., Hofmann, A.W., Brügmann, G., Batanova, V.G., Kuzmin, D.V., 2008. A quantitative link between recycling and osmium isotopes. Science 321, 536.
Stewart, A.J., van Westrenen, W., Schmidt, M.W., Günther, D., 2009. Minor element partitioning between fcc Fe metal and Fe–S liquid at high pressure: the role of crystal lattice strain. Earth Planet. Sci. Lett. 284, 302–309.
van Niekerk, D., Humayun, M., Keil, K., 2009. *In situ* determination of siderophile trace elements in EL3 meteorites. 40th Lunar and Planetary Science Conference, p. 2049.
Van Orman, J.A., Keshav, S., Fei, Y., 2008. High-pressure solid/liquid partitioning of Os, re and Pt in the Fe–S system. Earth Planet. Sci. Lett. 274, 250–257.
van Westrenen, W., Allan, N.L., Blundy, J.D., Purton, J.A., Wood, B.J., 2000. Atomistic simulation of trace element incorporation into garnets — comparison with experimental garnet-melt partitioning data. Geochim. Cosmochim. Acta 64, 1629–1639.
Wade, J., Wood, B.J., 2005. Core formation and the oxidation state of the Earth. Earth Planet. Sci. Lett. 236, 78–95.
Walker, D., 2000. Core participation in mantle geochemistry: geochemical Society Ingerson Lecture, GSA Denver, October 1999. Geochim. Cosmochim. Acta 64, 2897–2911.
Walker, D., Li, J., 2008. Partitioning of molybdenum to 60 kbar along a warped Fe–FeS liquidus. Chem. Geol. 248, 166–173.
Walker, R.J., Morgan, J.W., Horan, M.F., 1995. Osmium-187 enrichment in some plumes: evidence for core–mantle interaction? Science 269, 819–822.
Walker, R.J., Morgan, J.W., Beary, E.S., Smoliar, M.I., Czamanske, G.K., Horan, M.F., 1997. Applications of the ^{190}Pt–^{186}Os isotope system to geochemistry and cosmochemistry. Geochim. Cosmochim. Acta 61, 4799–4807.
Walker, R.J., McDonough, W.F., Honesto, J., Chabot, N.L., McCoy, T.M., Ash, R.D., Bellucci, J.J., 2008. Origin and chemical evolution of Group IVB iron meteorites. Geochim. Cosmochim. Acta 72, 2198–2216.
Warren, P.H., Ulff-Møller, F., Huber, H., Kallemeyn, G.W., 2006. Siderophile geochemistry of ureilites: a record of early stages of planetesimal core formation. Geochim. Cosmochim. Acta 70, 2104–2126.
Wood, B.J., Wade, J., Kilburn, M.R., 2008. Core formation and the oxidation state of the Earth: additional constraints from Nb, V and Cr partitioning. Geochim. Cosmochim. Acta 72, 1415–1426.